Tailoring the multiferroic properties in Ba0.85Ca0.15Zr0.1Ti0.9O3/La0.7Sr0.3MnO3 bilayer heterostructures using residual strain

Mingzhe Hu
Guizhou Minzu University

Rong Su (sr18034920313@163.com)
Guizhou Minzu University https://orcid.org/0000-0002-4677-7072

Chuanbin Wang
Wuhan University of Technology

Research Article

Keywords: Thickness, BCZT/LSMO, Residual strain, Multiferroic properties, Magnetoelectric effect

Posted Date: March 25th, 2021

DOI: https://doi.org/10.21203/rs.3.rs-339926/v1

Abstract

$Ba_{0.85}Ca_{0.15}Zr_{0.1}Ti_{0.9}O_3/La_{0.7}Sr_{0.3}MnO_3$ (BCZT/LSMO) bilayer multiferroic heterostructures with different BCZT layer thickness are fabricated by pulsed laser deposition technique. Structural characterization of XRD and TEM reveals the epitaxial growth of the bilayer heterostructures, whose residual strain reduces with increasing thickness. The room temperature multiferroic characteristics of the bilayer heterostructures are demonstrated by the simultaneously observed ferroelectric and ferromagnetic properties as well as the magnetoelectric effect. Due to the varying residual strain, the multiferroic properties of the bilayer heterostructures show strong dependence of the BCZT layer thickness, which significantly improves with increasing thickness. The largest magnetoelectric coefficient with α_{E31} value of 355.2 mV/cm·Oe is achieved in BCZT/LSMO bilayer heterostructures with BCZT layer thickness of 150 nm.

1. Introduction

Multiferroics are functional materials containing two or more basic ferro orderings (such as ferroelectric, ferromagnetic and so on), which can not only achieve the coexistence of multiple ferro orderings, but also produce a series of new physical effects stemming from the cross coupling between them [1–3]. Among them, the coupling effect between the ferroelectric ordering and ferromagnetic ordering that is known as the magnetoelectric (ME) coupling effect can realize the mutual regulation between electric field and magnetic field, which provides a new design freedom for the development and utilization of next generation multifunctional magnetoelectric devices based on charge order and spin order, and shows an attractive application prospect [4–6].

So far, very few single-phase multiferroics have been discovered, and it is difficult to obtain significant ME coupling effect at room temperature, which limits its practical application prospect [7, 8]. In contrast, most of the multi-phase composite multiferroics can achieve the strong ME coupling effect far greater than single-phase multiferroics at room temperature, which simultaneously display better design and preparation flexibility, and therefore have become one of the research hotspots in the field of multiferroic materials [9–11]. Initially, researches on multiferroic ME composites have mainly focused on the bulk materials. However, with the deepening of the study, researchers found that the interface cracks or interdiffusion during the fabrication process of bulk ME composites is very difficult to overcome, which significantly degrades the interface bonding quality and thereby results in the weak ME coefficient far lower than the theoretical value [12–14]. As a result, more and more ME composite thin films have been developed due to the rapid development of advanced thin film growth techniques and theoretical computing science. Compared to the bulk ME composites, ME composite thin films display many inherent advantages such as more freedom and flexibility in design, more effective interface coupling at nanoscale and more compatible with modern microelectronic integrated circuit technology [15–17].

The ME composite thin films with alternating layer structure show more prospect due to their low leakage current and sufficient polarization [18]. In general, strain-mediated ME coupling mechanism is the most

widely recognized in layered ME thin films, which means that strong ME effect is easier to achieve in layered ME thin films composed of ferroelectric phase with large piezoelectric effect and ferromagnetic phase with high magnetostriction. Otherwise, lead-based piezoelectric materials are currently the most commonly used ferroelectric phase due to their excellent piezoelectric properties. A series of layered ME thin films based on lead-based piezoelectric materials as the ferroelectric phase have been developed, such as $Pb(Zr_{0.52}Ti_{0.48})O_3/La_{0.7}Sr_{0.3}MnO_3$ [19] and $ZnFe_2O_4/0.67Pb(Mg_{1/3}Nb_{2/3})O_3$-$0.33PbTiO_3$ [20], which showed good multiferroic performances. However, pursuing lead-free multiferroic ME materials is the future development direction because of the damages of lead-based materials to the environment.

$Ba_{0.85}Ca_{0.15}Zr_{0.1}Ti_{0.9}O_3$ (BCZT) is regarded as one of the most promising lead-free piezoelectric materials due to its equivalent piezoelectric properties to lead-based piezoelectric materials and environmentally-friendly nature [21], and thereby is chosen as the ferroelectric phase in this paper. Furthermore, perovskite lanthanum manganite $La_{0.7}Sr_{0.3}MnO_3$ (LSMO) has attracted ever increasing attention as a ferromagnetic phase material because of its double exchange mediated ferromagnetism metallic conductivity with ferromagnetic Curie temperature (~ 370K) well above room temperature, which is thus selected as the ferromagnetic phase [22, 23]. And the LSMO thin film was deposited not only as a ferromagnetic layer but also as a bottom electrode. As far as we know, few works have been conducted on ME heterostructure consists of BCZT ferroelectric layer and LSMO ferromagnetic layer. Besides, extensive reports found that the film thickness shows great influence on the residual strain and multiferroic properties of the ME heterostructures [24, 25]. As a consequence, we present a detail study on the effect of thickness on residual strain and multiferroic properties in $Ba_{0.85}Ca_{0.15}Zr_{0.1}Ti_{0.9}O_3/La_{0.7}Sr_{0.3}MnO_3$ (BCZT/LSMO) bilayer multiferroic heterostructures.

2. Experimental

LSMO thin films with thickness of 100 nm and then BCZT thin films with thickness of 50 nm, 100 nm and 150 nm were grown on (100)-oriented $SrTiO_3$ (STO) single crystal substrates by pulsed laser deposition (PLD, PLVD-362, EOR), to form the BCZT/LSMO bilayer multiferroic heterostructures. A KrF excimer laser with a 248 nm wavelength and 10 Hz pulse rate was used during the deposition process. The growth temperature and laser energy of the LSMO and BCZT thin films were both fixed at 650°C and 300 mJ, while the oxygen pressure were 20 Pa and 10 Pa, respectively.

Structure characterization of the BCZT/LSMO bilayer heterostructures was performed on a four-circle high resolution x-ray diffraction (HRXRD, Empyrean, PANalytical). Transmission electron microscopy (TEM, Titan Themis 200, FEI) was adopted to characterize the cross-sectional microstructure and element distribution. The piezoelectric response was recorded by piezoresponse force microscope (PFM, Dimension Icon Atomic Force Microscope, Bruker). The ferroelectric hysteresis loops and leakage current curves were measured by ferroelectric tester (Premier II, Radiant). An Agilent E4980A impedance analyzer was used to measure the room temperature dielectric constant. Room temperature ferromagnetic properties were measured using a physical property measurement system (PPMS, LakeShore7404,

Quantum Design). A Quantum Design ME measurement system was employed to test the room temperature transverse ME coefficient (α_{E31}) of the bilayer heterostructures with the applied magnetic field parallel to the film surface at 1 kHz.

3. Results And Discussion

3.1. Structure analysis

Figure 1 (a) shows the HRXRD patterns of the BCZT/LSMO bilayer heterostructures with different thickness. It can be seen that the diffraction peaks of all bilayer heterostructures grow preferentially along the (*l*00) diffraction peaks of the STO substrate without any impurity phases, which are highly consistent with the orientation of the STO substrate. In order to obtain the variation of lattice constant and residual strain of the bilayer heterostructures with thickness, the reciprocal space mapping (RSM) around the asymmetric (103) reflections are recorded as shown in Fig. 1 (b). The overall features of the asymmetric RSM (103) reflections for bilayer heterostructures with different thickness suggest that the fully strained LSMO layer is under an in-plane tensile strain and the partially relaxed BCZT layer is subjected to an in-plane compressive strain [26]. Besides, the enhanced intensity of the BCZT (103) reflections indicates the improving crystallinity of the BCZT layer thin film with increasing thickness. The lattice constants of the BCZT layer thin films for all bilayer heterostructures along with the corresponding residual strain are determined from the asymmetric RSM (103) reflections. The horizontal RSM peak position determines the in-plane lattice constant *a* while the vertical one corresponds to the out-of plane lattice constant *c*. Table 1 summarizes the *a* and *c* of the BCZT layers for BCZT/LSMO bilayer heterostructures with different thickness. When the thickness of the BCZT layer increases from 50 nm to 150 nm, its lattice constant *a* increases from 4.0010 to 4.0057 and *c* reduces from 4.0485 to 4.0366. In addition, the equations $\varepsilon_a = (a - a_0)/a_0$ and $\varepsilon_c = (c - c_0)/c_0$ were used to calculate the in-plane (ε_a) and out-of-plane (ε_c) residual strains of the BCZT layers, respectively. Where a_0 and c_0 are lattice constant of the BCZT ceramic ($a_0 = 4.007$ and $c_0 = 4.025$) [21]. The calculated values of residual strain are listed in Table 1. It can be seen that both the in-plane and out-of-plane residual strain of the bilayer heterostructures gradually decrease with increasing BCZT layer thickness.

Table 1
Structure parameters and residual strains of the BCZT/LSMO bilayer heterostructures with different thickness.

Thickness/nm	*a*/Å	*c*/Å	ε_a/%	ε_c/%
50	4.0010	4.0485	-0.15	0.58
100	4.0025	4.0418	-0.11	0.42
150	4.0051	4.0366	-0.05%	0.29

In order to further characterize the crystallinity and micro-area structure of the BCZT/LSMO bilayer heterostructures, the sample with BCZT layer thickness of 150 nm is selected for TEM characterization. As can be seen from the cross-sectional TEM image in Fig. 2, the uniform thickness of the bottom LSMO layer and the top BCZT layer presents a clear and distinct interface. The energy dispersive spectrometer (EDS) element mapping of the bilayer heterostructure based on white square displays the evident boundaries across the BCZT-LSMO and LSMO-STO interfaces, demonstrating the evenly distributed chemical elements without any interface element diffusion phenomenon. The high-resolution TEM (HRTEM) and corresponding selected area electron diffraction (SAED) images of the BCZT-LSMO and LSMO-STO interfaces are also shown in Fig. 2. We can observe that both the two interfaces are very clear and sharp with almost no defects, and the corresponding SAED spots are orderly arranged. Furthermore, the diffraction spots at the BCZT-LSMO interface are almost coincided, while those at the LSMO-STO interface are completely overlapped. Above all, the BCZT/LSMO bilayer heterostructure epitaxially grow on STO substrate and show excellent crystallinity.

3.2. Electrical properties

Figures 3 (a) and (b) show the local piezoresponse hysteresis loops of phase and amplitude for the BCZT/LSMO bilayer heterostructures with different thickness, respectively. The approximately 180° reversible switching of the piezoresponse phase and well-defined butterfly loops of the piezoresponse amplitude indicate the good switching behavior of the BCZT/LSMO bilayer heterostructures with different thickness. It should be noted that the common asymmetry behavior in the amplitude-voltage butterfly loops of all samples should be stemmed from the electrode self-poling effect [27]. Meanwhile, the effective piezoelectric constants (d_{33}) of the bilayer heterostructures with different thickness are displayed in Fig. 3 (c), which were determined from the amplitude-voltage loops. The calculated values of d_{33} are 31.4 pm/V, 38.7 pm/V and 47.2 pm/V for BCZT/LSMO bilayer heterostructures with 50 nm, 100 nm and 150 nm BCZT layer thickness, respectively. The piezoresponse of the bilayer heterostructures enhances with the increase of BCZT layer thickness mainly because of the decreased residual strain. It has been reported that the ferroelectric domain pinning would be more severe under larger residual strain, and in turn weakens the polarization switching [28]. Therefore, the BCZT/LSMO bilayer heterostructure with 150 nm BCZT layer exhibits the strongest piezoresponse due to its smallest residual strain.

Figure 4 (a) presents the room temperature ferroelectric hysteresis loops of the BCZT/LSMO bilayer heterostructures with different thickness at 1 kHz. The well-shaped ferroelectric hysteresis loops indicate the ferroelectric nature of all bilayer heterostructures. Besides, the determined remanent polarizations (P_r) are 7.5 μC/cm^2, 12.3 μC/cm^2 and 18.6 μC/cm^2 for BCZT/LSMO bilayer heterostructures with 50 nm, 100 nm and 150 nm BCZT layer, respectively, while their corresponding coercive electric fields (E_C) are 199.2 kV/cm, 193.7 kV/cm and 181.5 kV/cm. The leakage curves in Fig. 4 (b) suggest that the increase in BCZT layer thickness is beneficial to reduce the leakage current of the bilayer heterostructures. Therefore, the enhancement in P_r of the bilayer heterostructures with increasing BCZT layer thickness should be ascribed to the improved crystallinity of the BCZT layer and the reduced leakage current of the bilayer heterostructures, which could lead to more sufficient polarization. Furthermore, the decrease in E_C with

increasing BCZT layer thickness may be explained by the passive interfacial layer effect. This seems to be a very common phenomenon in ME bilayer thin films, which has also been found in many similar works [24, 29–31]. The passive interfacial layer, exists at the BCZT/LSMO interface stemming from the misfit dislocation, could hamper ferroelectric domain switching [32, 33]. The increase in BCZT layer thickness would reduce the portion of the passive interfacial layer in the bilayer heterostructures, and therefore the BCZT/LSMO bilayer heterostructures with thicker BCZT layer display the smaller E_C.

The frequency dependence of dielectric constant (ε_r) for the BCZT/LSMO bilayer heterostructure with different thickness measured at room temperature is displayed in Fig. 5. It can be clearly observed that the ε_r of the BCZT/LSMO bilayer heterostructures reduces as the frequency increases, which is attributed to the lack of ability of dipoles to follow the rapidly changing electric field at higher frequency [34]. Moreover, the ε_r values at 1 kHz are 452.1, 608.2 and 746.4 for the BCZT/LSMO bilayer heterostructures with 50 nm, 100 nm and 150 nm BCZT layer thickness, respectively. The decrease in ε_r with increasing BCZT layer thickness should be due to the reducd in-plane compressive strain in the BCZT layer. Some previous works have noted that the in-plane two-dimensional compression in the ferroelectric thin films could alter the ionic positions and vibrations that coupled to the polarization mechanism, and finally weaken the dielectric constant of the ferroelectric materials [35, 36].

3.3. Ferromagnetic and magnetoelectric properties

Figure 6 shows the temperature dependence on magnetization for the BCZT/LSMO bilayer heterostructures with different thickness, which are measured at 1000 Oe with a magnetic field applied perpendicular to the polarization direction. An evident ferromagnetic-paramagnetic phase transition can be observed in all bilayer heterostructures. Furthermore, the maximum magnetization of the bilayer heterostructures increases with increasing thickness. The phase transition temperature, also known as the Curie temperature (T_C), is defined as the peak temperature of dM/dT. The inset presents the temperature dependent derivative of magnetization (dM/dT). The T_C of the bilayer heterostructures with 50 nm, 100nm and 150 nm BCZT layer is around 310.5K, 320.1K and 326.3K, respectively, suggesting that the increases in BCZT layer thickness would enhance the Curie temperature of the bilayer heterostructures.

In order to further study the ferromagnetic properties of the BCZT/LSMO bilayer heterostructures, the room temperature magnetic field dependence of magnetization for the bilayer heterostructures with different thickness are measured, as shown in Fig. 7. The well-behaved ferromagnetic hysteresis loops demonstrate the ferromagnetic nature of the bilayer heterostructures with different thickness. At the same time, it can be seen that the saturated magnetization of the bilayer heterostructures improves with increasing BCZT layer thickness. According to the partially enlarged loops shown in the inset, the increase in BCZT layer thickness causes the coercive magnetic field of the bilayer heterostructures increases. The ferromagnetic properties study reveals that the increase in BCZT layer thickness could lead to a larger magnetization of the bilayer heterostructures. Similar phenomena have also been found in $PbZr_{0.52}Ti_{0.48}O_3/La_{0.67}Sr_{0.33}MnO_3$ [30] and $CoFe_2O_4/PbZr_{0.52}Ti_{0.48}O_3$ [37] bilayer thin films in which

improved magnetization was obtained in thicker ferroelectric layer that grown on the top of ferromagnetic layer with fixed thickness. And the enhancement in magnetization may be related to the interface coupling effect between the BCZT and LSMO layers. Nevertheless, it needs further study to figure out the BCZT layer thickness effect on the oxidation states of Mn in LSMO layer [24].

Figure 8 shows the magnetic field dependence of the transverse ME coefficient (α_{E31}) for BCZT/LSMO bilayer heterostructures with different thickness, and the magnetic field is applied parallel to the film surface at room temperature. It can be clearly observed that the values of α_{E31} for all samples gradually increase with increasing magnetic field, and then reaches the maximum values at a certain magnetic field where the magnetostriction of the LSMO layer get saturated. The certain magnetic field of all bilayer heterostructures are both around 1500 Oe and have nothing to do with the change of BCZT layer thickness. Furthermore, the maximum values of α_{E31} for BCZT/LSMO bilayer heterostructures with 50 nm, 100 nm and 150 nm BCZT layer thickness are 183.2 mV/cm·Oe, 283.7 mV/cm·Oe and 355.2 mV/cm·Oe, respectively.

In the stress/strain modulated multiferroic heterostructures, the ferromagnetic phase produces and transfers stress/strain to the adjacent ferroelectric phase through the elastic coupling at the interface, inducing the positive piezoelectric effect, which can be depicted as a product of piezoelectric effect and magnetostrictive effect:

$$\alpha_{E31} = \frac{\text{magnetic field}}{\text{stress/str ain}} \times \frac{\text{stress/str ain}}{\text{ferroelect ric polarizati on}} \qquad (1)$$

The α_{E31} could be affected by the ratio of ferroelectric phase to ferromagnetic phase, the direction of the ferroelectric polarization, as well as the resistivity of ferromagnetic phase (which determines the maximum applied electric field intensity). In addition, the residual stress, grain boundary, dislocation and substrate clamping can hinder the elastic coupling. Thus, the smaller the residual strain of the BCZT layer is, the larger the α_{E31} of the bilayer heterostructures becomes, since only the residual stress is tailored in terms of BCZT thickness in all epitaxially grown interfaces.

Moreover, the ME coefficient of the BCZT/LSMO bilayer heterostructures is larger than that of the $BaTiO_3/La_{0.7}Sr_{0.3}MnO_3$ (BTO/LSMO) bilayer heterostructures (140-213 mV/cm·Oe) [38, 39]. The enhancement in ME coupling effect should be resulted from the stronger piezoelectric effect of the BCZT than BTO ferroelectric phase according to equation (1).

4. Conclusions

In summary, BCZT/LSMO bilayer multiferroic heterostructures with different BCZT layer thickness were deposited on STO single crystal substrates by pulsed laser deposition, so as to investigate the thickness

effect on residual strain and multiferroic properties. XRD and TEM analysis confirm the epitaxial growth of the bilayer heterostructures and the decreased residual strain with increasing BCZT thickness. The simultaneously observation of ferroelectric and ferromagnetic properties as well as magnetoelectric effect at room temperature verifies the multiferroic nature of the bilayer heterostructures. The residual strain in terms of BCZT layer thickness has a great influence on multiferroic properties of the bilayer heterostructures. Results show that the multiferroic properties enhance with increasing BCZT thickness. BCZT/LSMO bilayer heterostructure with BCZT layer thickness of 150 nm exhibits the strongest magnetoelectric effect with α_{E31} value of 355.2 mV/cm·Oe.

Declarations

Acknowledgement

This work is financially supported by the National Natural Science Foundation of China (51972252, 51567017), the Key Project of the Education Department of Guizhou Province (KY2021045), the Construction Project of Characteristic Key Laboratory in Guizhou Colleges and Universities (KY2021003), the Fundamental Research Funds for the Central Universities (WUT: 2019□029) and the National Science Foundation of Guizhou Province (No.2021199).

Competing financial interests declaration

The authors hereby formally declare no competing financial interests in the present article “Tailoring the multiferroic properties in $Ba_{0.85}Ca_{0.15}Zr_{0.1}Ti_{0.9}O_3/La_{0.7}Sr_{0.3}MnO_3$ bilayer heterostructures using residual strain”.

References

[1] N.A. Spaldin, R. Ramesh, Advances in magnetoelectric multiferroics, Nat. Mater. 18 (2019) 203. https://doi.org/10.1038/s41563-018-0275-2

[2] W. Kleemann, Multiferroic and magnetoelectric nanocomposites for data processing, J. Phys. D Appl. Phys. 50 (2017) 223001. https://doi.org/10.1088/1361-6463/aa6c04

[3] C.W. Nan, J.M. Liu, Multiferroics: a beautiful but challenging multi-polar world, Nat. Sci. Rev. 6 (2019) 620-620. https://doi.org/10.1093/nsr/nwz093

[4] M. Bibes, A. Barthélémy, Multiferroics: Towards a magnetoelectric memory, Nat. Mater. 7 (2008) 425-426. https://doi.org/10.1093/nsr/nwz093

[5] Y. Wang, J. Li, D. Viehland, Magnetoelectrics for magnetic sensor applications: status, challenges and perspectives, Mater. Today 17 (2014) 269-275. https://doi.org/10.1016/j.mattod.2014.05.004

[6] N. Kumar, A. Shukla, N. Kumar, R.N.P. Choudhary, Design and development of bismuth ferrite based environmental friendly multiferroic for devices, Mater. Today Proc. 18 (2019) 638-646. https://doi.org/10.1016/j.matpr.2019.06.458

[7] C. Lu, M. Wu, L. Lin, J.M. Liu, Single-phase multiferroics: new materials, phenomena, and physics, Nat. Sci. Rev. 6 (2019) 653-668. https://doi.org/10.1093/nsr/nwz091

[8] M. Fiebig, T. Lottermoser, D. Meier, M. Trassin, The evolution of multiferroics, Nat. Rev. Mater. 1 (2016) 16046. https://doi.org/10.1038/natrevmats.2016.46

[9] H. Palneedi, V. Annapureddy, S. Priya, J. Ryu, Status and perspectives of multiferroic magnetoelectric composite materials and applications, Actuators, 5 (2016) 9. https://doi.org/10.3390/act5010009

[10] W. Eerenstein, N. Mathur, J.F. Scott, Multiferroic and magnetoelectric materials, Nature 442 (2006) 759. https://doi.org/10.1038/nature05023

[11] M. Naveed-Ul-Haq, S. Webers, H. Trivedi, S. Salamon, H. Wende, M. Usman, A. Mumtaz, V.V. Shvartsman, D.C. Lupascu, Effect of substrate orientation on local magnetoelectric coupling in bi-layered multiferroic thin films, Nanoscale 10 (2018) 20618-20627. https://doi.org/10.1039/C8NR06041J

[12] S. Li, C. Wang, Q. Shen, L. Zhang, Enhanced dielectric properties in $Ba_{0.85}Ca_{0.15}Zr_{0.10}Ti_{0.90}O_3/La_{0.67}Ca_{0.33}MnO_3$ laminated composite, Script. Mater. 144 (2018) 40-43. https://doi.org/10.1016/j.scriptamat.2017.09.044

[13] C.S. Park, S. Priya, Cofired magnetoelectric laminate composites, J. Am. Ceram. Soc. 94 (2011) 1087-1095. https://doi.org/10.1111/j.1551-2916.2010.04213.x

[14] W.S. Rosa, M. Venet, Exploring the processing conditions to optimize the interface in 2–2 composites based on $Pb(Zr,Ti)O_3$ and $NiFe_2O_4$, Ceram. Int. 42 (2016) 7980-7986. https://doi.org/10.1016/j.ceramint.2016.01.196

[15] Z. Chu, M. PourhosseiniAsl, S. Dong, Review of multi-layered magnetoelectric composite materials and devices applications, J. Phys. D Appl. Phys. 51 (2018) 243001. https://doi.org/10.1088/1361-6463/aac29b

[16] C.A. Fernandes Vaz, U. Staub, Artificial multiferroic heterostructures, J. Mater. Chem. C 1 (2013) 6731. https://doi.org/10.1039/C3TC31428F

[17] J.M. Hu, C.G. Duan, C.W. Nan, L.Q. Chen, Understanding and designing magnetoelectric heterostructures guided by computation: progresses, remaining questions, and perspectives, NPJ Comput. Mater. 3 (2017) 1-21. https://doi.org/10.1038/s41524-017-0020-4

[18] C. Deng, Y. Zhang, J. Ma, Y. Lin, C.W. Nan, Magnetoelectric effect in multiferroic heteroepitaxial $BaTiO_3$-$NiFe_2O_4$ composite thin films. Acta Mater. 56 (2008) 405-412.

https://doi.org/10.1016/j.actamat.2007.10.004

[19] D. Mukherjee, M. Hordagoda, P. Lampen, M.H. Phan, H. Srikanth, S. Witanachchi, P. Mukherjee, Simultaneous enhancements of polarization and magnetization in epitaxial $Pb(Zr_{0.52}Ti_{0.48})O_3/La_{0.7}Sr_{0.3}MnO_3$ multiferroic heterostructures enabled by ultrathin $CoFe_2O_4$ sandwich layers, Phys. Rev. B 91 (2015) 054419. https://doi.org/10.1103/PhysRevB.91.054419

[20] T. Garg, A. Kulkarni, N. Venkataramani, Room-temperature magneto-dielectric response in multiferroic $ZnFe_2O_4$/PMN-PT bilayer thin films, Smart. Mater. Struct. 25 (2016) 085032. https://doi.org/10.1088/0964-1726/25/8/085032

[21] W. Liu, X. Ren, Large piezoelectric effect in Pb-free ceramics, Phys. Rev. Lett. 103 (2009) 257602. https://doi.org/10.1103/PhysRevLett.103.257602

[22] C. Vaz, J. Hoffman, Y. Segal, J. Reiner, R. Grober, Z. Zhang, C. Ahn, F.J Walker, Origin of the magnetoelectric coupling effect in $Pb(Zr_{0.2}Ti_{0.8})O_3/La_{0.8}Sr_{0.2}MnO_3$ multiferroic heterostructures, Phys. Rev. Lett. 104 (2010) 127202. https://doi.org/10.1103/PhysRevLett.104.127202

[23] J.M. Yan, G.-Y. Gao, Y.K. Liu, F.F. Wang, R.K. Zheng, Electric-field control of electronic transport properties and enhanced magnetoresistance in $La_{0.7}Sr_{0.3}MnO_3/0.5BaZr_{0.2}Ti_{0.8}O_3$-$0.5Ba_{0.7}Ca_{0.3}TiO_3$ lead-free multiferroic structures, J. Appl. Phys. 122 (2017) 134102. https://doi.org/10.1063/1.4990513

[24] S. Li, C. Wang, Q. Shen, L. Zhang, Residual Strain-mediated multiferroic properties of $Ba_{0.85}Ca_{0.15}Zr_{0.9}Ti_{0.1}O_3/La_{0.67}Ca_{0.33}MnO_3$ epitaxial heterostructures, ACS Appl. Mater. Int. 11 (2019) 30376-30383. https://doi.org/10.1021/acsami.9b05747

[25] K. Liang, P. Zhou, Z.J. Ma, Y.J. Qi, Z.H. Mei, T.J. Zhang, Multiferroic magnetoelectric coupling effect of bilayer $La_{1.2}Sr_{1.8}Mn_2O_7/PbZr_{0.3}Ti_{0.7}O_3$ complex thin film. Phys.s Lett. A, 381 (2017) 1504-1509. https://doi.org/10.1016/j.physleta.2017.02.029

[26] R.J. Kennedy, P.A. Stampe, Reciprocal space mapping of epitaxial MgO films on $SrTiO_3$, J. Cryst. Growth. 207 (1999) 200-205. https://doi.org/10.1016/S0022-0248(99)00371-1

[27] Q. Lin, D. Wang, Z.G. Chen, W. Liu, S. Li, Interfaces, Periodicity dependence of the built-in electric field in $(Ba_{0.7}Ca_{0.3})TiO_3/Ba(Zr_{0.2}Ti_{0.8})O_3$ ferroelectric superlattices, ACS Appl. Mater. Int. 7 (2015) 26301-26306. https://doi.org/10.1021/acsami.5b08943

[28] T.A. Berfield, R.J. Ong, D.A. Payne, N.R. Sottos, Residual stress effects on piezoelectric response of sol-gel derived lead zirconate titanate thin films, J. Alloy. Compd. 101 (2007) 24102-24100. https://doi.org/10.1063/1.2422778

[29] T. Li, K. Li, Z. Hu, Thickness and frequency dependence of magnetoelectric effect for epitaxial $La_{0.7}Sr_{0.3}MnO_3/BaTiO_3$ bilayer, J. Alloy. Compd. 592 (2014) 266-270.

https://doi.org/10.1016/j.jallcom.2014.01.021

[30] D. Barrionuevo, N. Ortega, A. Kumar, R. Chatterjee, J. Scott, R.J. Katiyar, Thickness dependent functional properties of $PbZr_{0.52}Ti_{0.48}O_3/La_{0.67}Sr_{0.33}MnO_3$ heterostructures, J. Appl. Phys. 114 (2013) 234103. https://doi.org/10.1063/1.4848017

[31] R. Gupta, S. Chaudhary, R.K. Kotnala, Interfacial charge induced magnetoelectric coupling at $BiFeO_3/BaTiO_3$ bilayer interface, ACS Appl. Mater. Int. 7 (2015) 8472-8479. https://doi.org/10.1021/am509055f

[32] A.K. Tagantsev, G. Gerra, Interface-induced phenomena in polarization response of ferroelectric thin films, J. Appl. Phys. 100 (5) (2006) 051607. https://doi.org/10.1063/1.2337009

[33] J. Wang, Z. Li, J. Wang, H. He, C.J. Nan, Effect of thickness on the stress and magnetoelectric coupling in bilayered $Pb(Zr_{0.52}Ti_{0.48})O_3$-$CoFe_2O_4$ films, J. Appl. Phys. 117 (2015) 044101. https://doi.org/10.1063/1.4906407

[34] J. Rani, V.K. Kushwaha, J. Kolte, C.V. Tomy, Strong magnetoelectric effect in pulse laser deposited $[Ba(Zr_{0.2}Ti_{0.8})O_3$-$0.5(Ba_{0.7}Ca_{0.3})TiO_3]/CoFe_2O_4$ bilayer thin film, J. Am. Ceram. Soc. 101 (2018) 5651-5658. https://doi.org/10.1111/jace.15882

[35] W. Chang, C.M. Gilmore, W.J. Kim, J.M. Pond, S.W. Kirchoefer, S.B. Qadri, D.B. Chirsey, J.S. Horwitz, Influence of strain on microwave dielectric properties of (Ba, Sr)TiO_3 thin films, J. Appl. Phys. 87 (2000) 3044-3049. https://doi.org/10.1063/1.372297

[36] R.F. Brown, Effect of Two-dimensional mechanical stress on the dielectric properties of poled ceramic barium titanate and lead zirconate titanate, Can. J. Phys. 39 (2011) 741-753. https://doi.org/10.1139/p61-082

[37] C.H. Sim, A.Z.Z. Pan, J. Wang, Thickness and Coupling Effects in Bilayered Multiferroic $CoFe_2O_4/Pb(Zr_{0.52}Ti_{0.48})O_3$ Thin Films, J. Appl. Phys. 103 (2008) 475-496. https://doi.org/10.1063/1.2940014

[38] T. Li, F. Zhang, H. Fang, K. Li, F. Yu, The magnetoelectric properties of $La_{0.7}Sr_{0.3}MnO_3/BaTiO_3$ bilayers with various orientations, J. Alloy. Compd. 560 (2013) 167-170. https://doi.org/10.1016/j.jallcom.2013.01.143

[39] T. Li, Z. Hu, M. Zhang, K. Li, D. Yu, H. Yan, Frequency dependence of magnetoelectric effect in epitaxial $La_{0.7}Sr_{0.3}MnO_3/BaTiO_3$ bilayer film, Appl. Sur. Sci. 258 (2012) 4558-4562. https://doi.org/10.1016/j.apsusc.2012.01.027

Figures

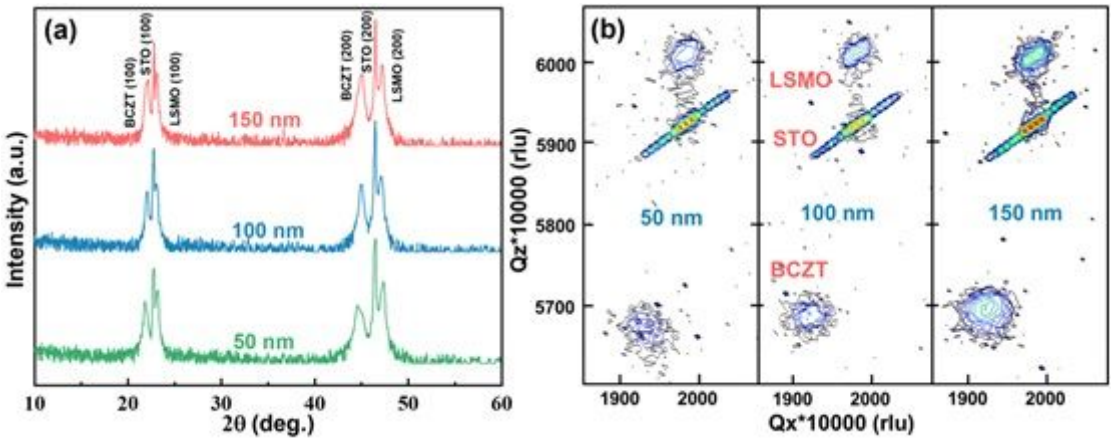

Figure 1

(a) HRXRD and (b) RSM results of the BCZT/LSMO bilayer heterostructures with different thickness.

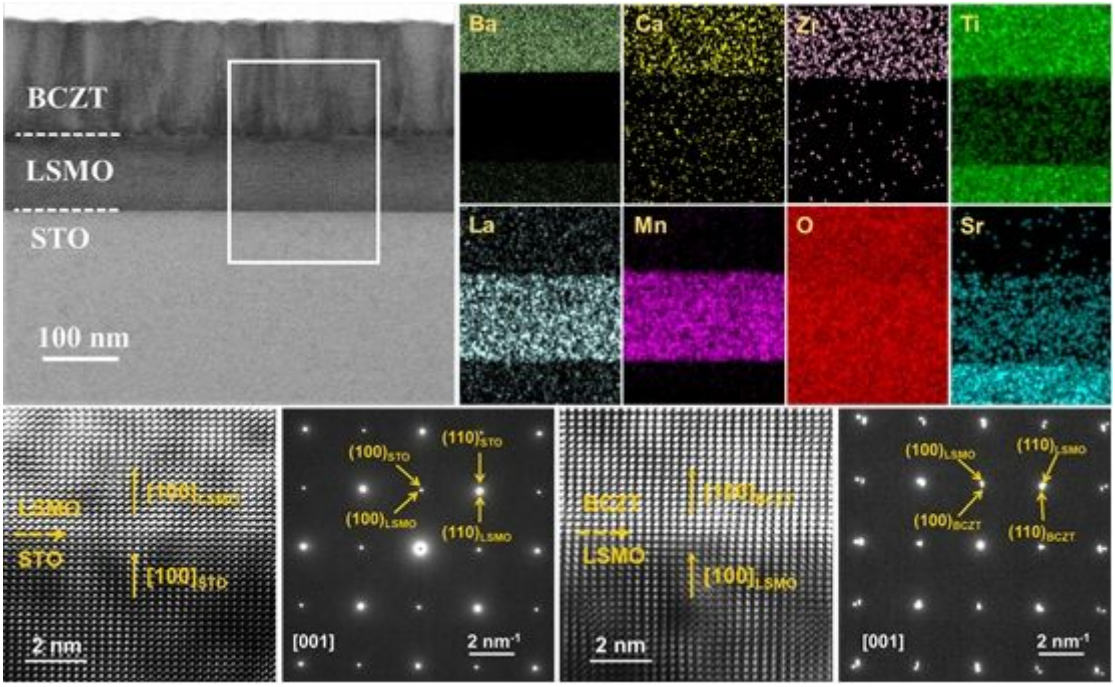

Figure 2

Cross-sectional TEM, EDS element mapping, HRTEM and SAED images of the BCZT/LSMO bilayer heterostructure with BCZT layer thickness of 150 nm.

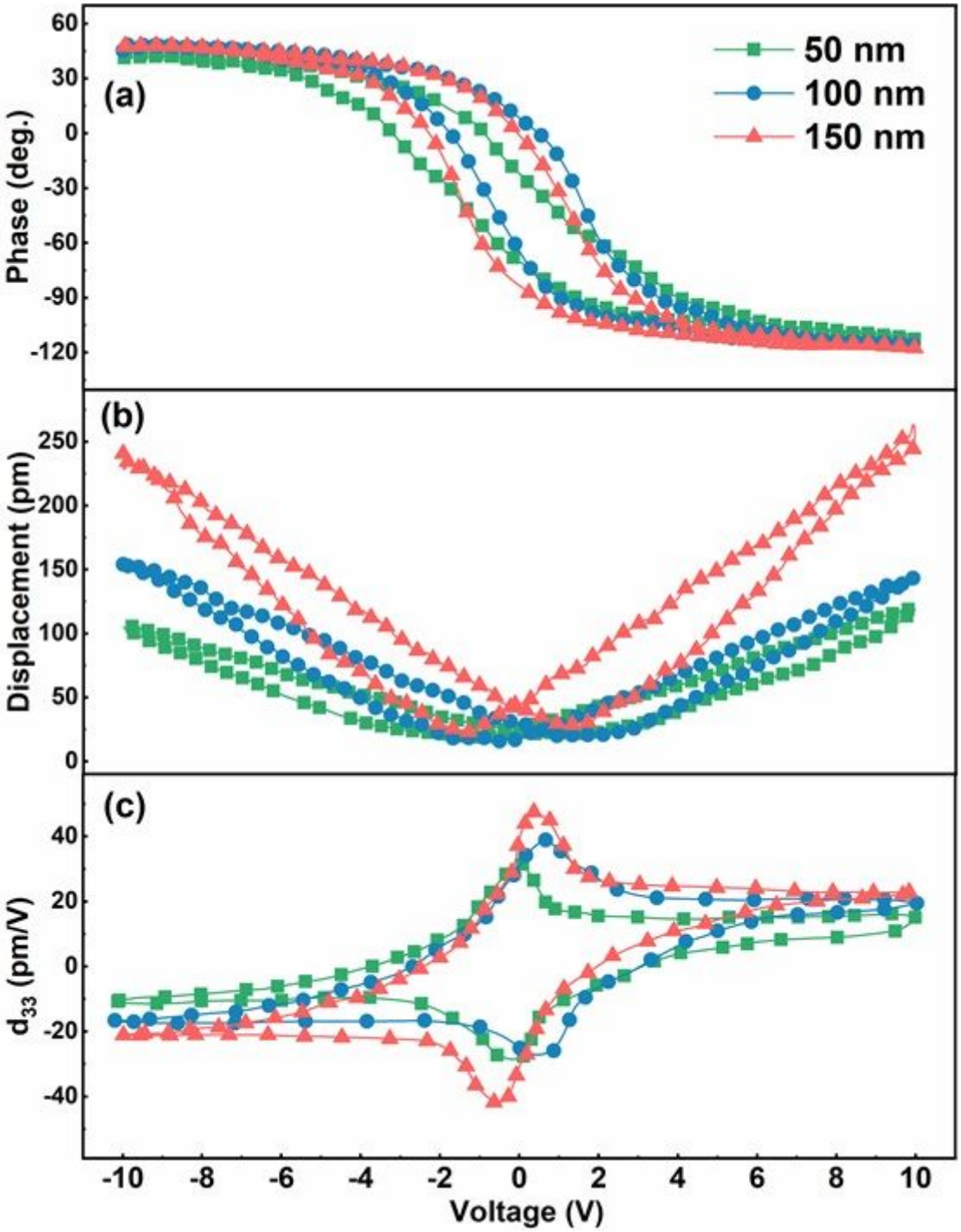

Figure 3

Local piezoresponse (a) phase, (b) amplitude and (c) effective d33 hysteresis loops of the BCZT/LSMO bilayer heterostructures with different thickness.

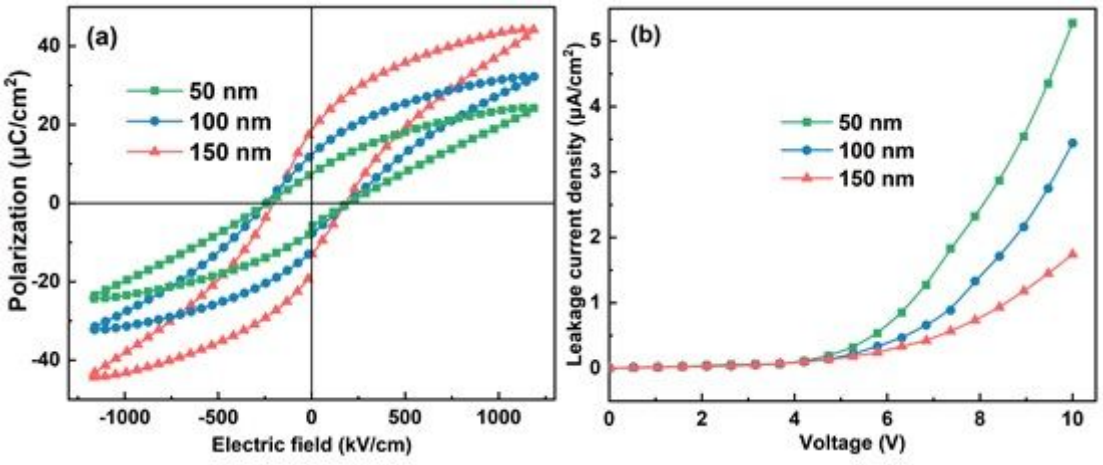

Figure 4

(a) Ferroelectric hysteresis loops and (b) leakage current density of the BCZT/LSMO bilayer heterostructures with different thickness.

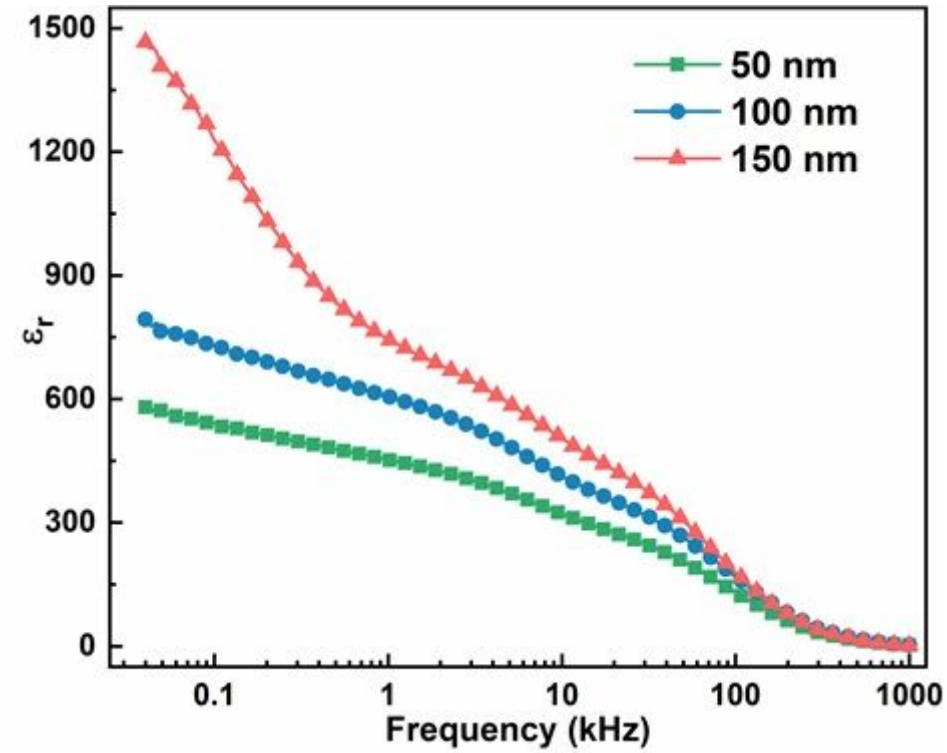

Figure 5

Frequency dependence of dielectric constant for BCZT/LSMO bilayer heterostructures with different thickness.

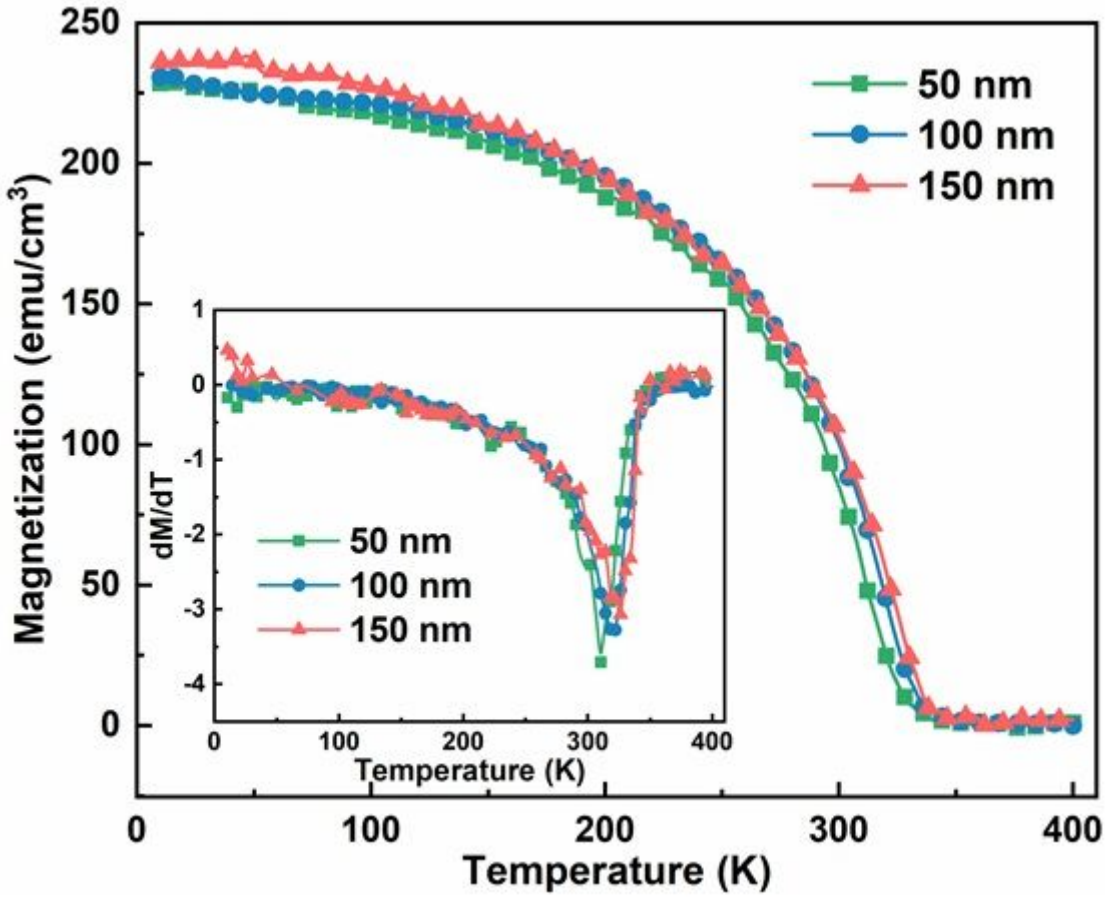

Figure 6

Temperature dependent magnetization of the BCZT/LSMO bilayer heterostructures with different thickness. The inset presents the temperature dependent derivative of magnetization (dM/dT).

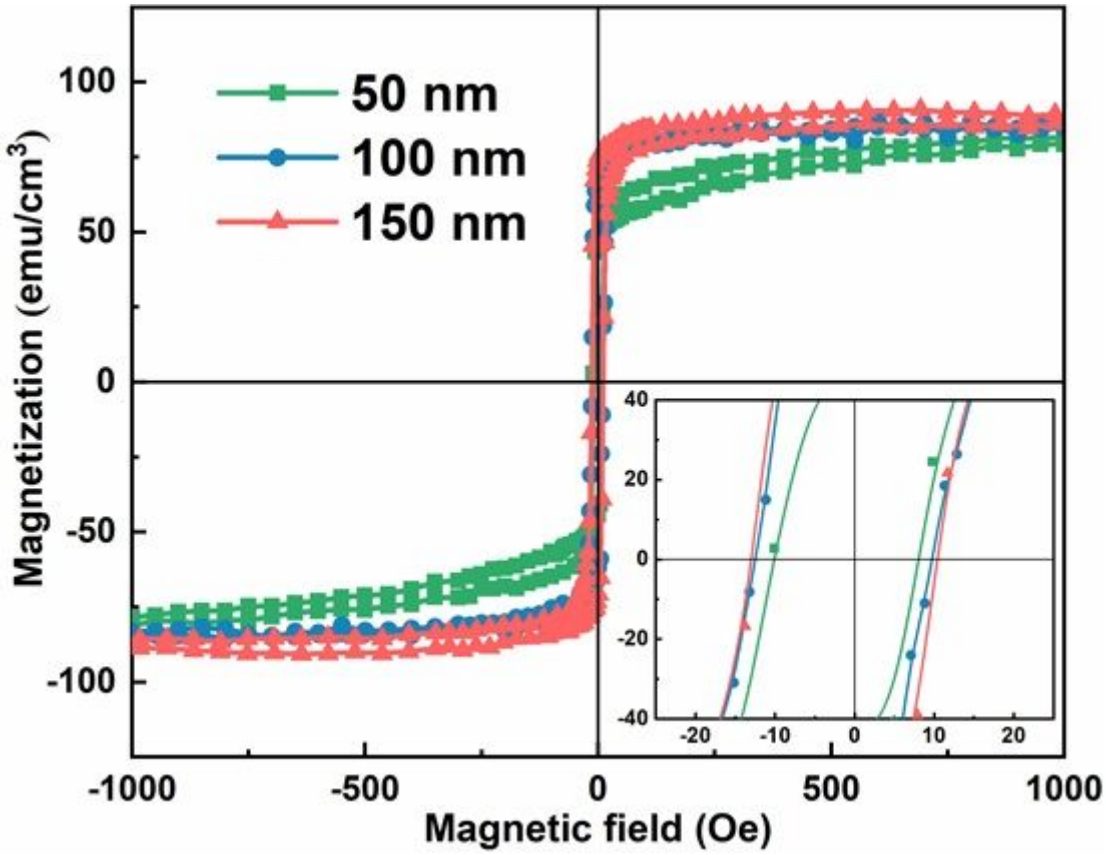

Figure 7

Ferromagnetic hysteresis loops of the BCZT/LSMO bilayer heterostructures with different thickness. The inset shows the partially enlarged loops.

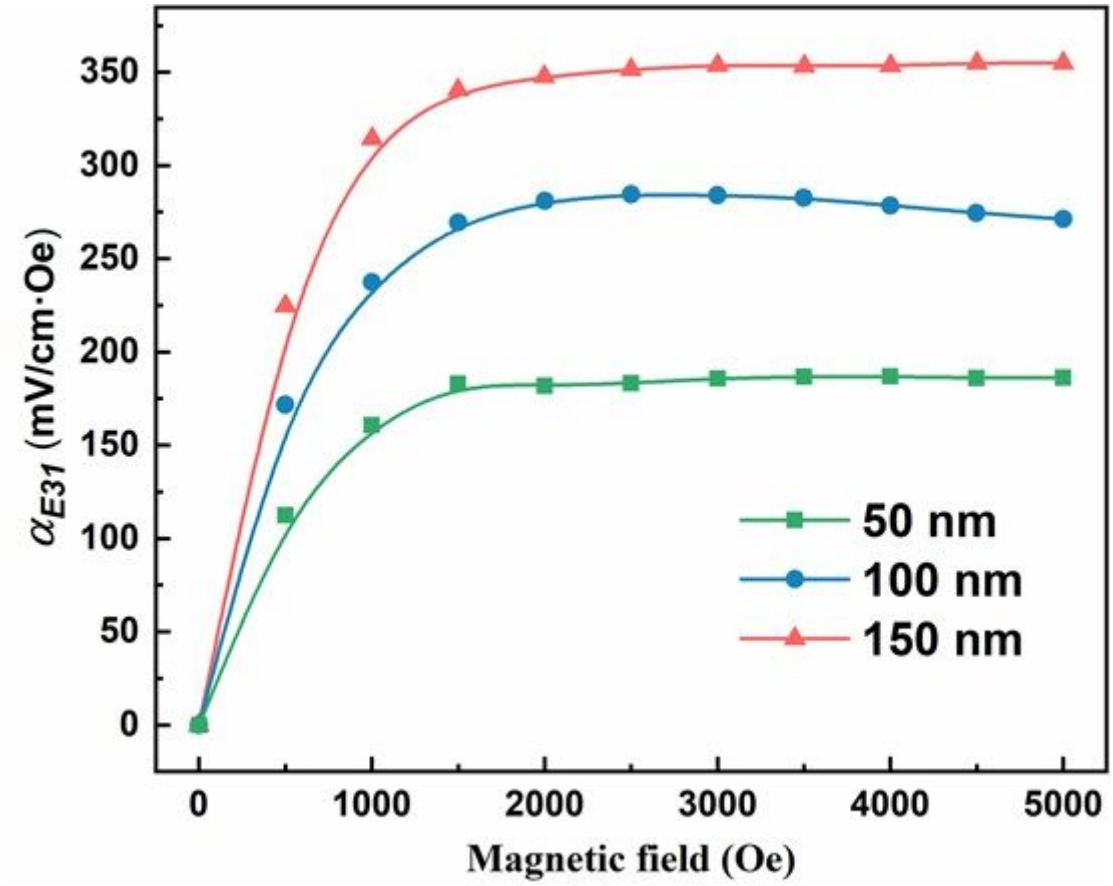

Figure 8

Magnetic field as a function of the ME coefficients for BCZT/LSMO bilayer heterostructures with different thickness.